



Cite this: *New J. Chem.*, 2015, 39, 953

# The electrochemical synthesis of Pt particles on ZrO<sub>2</sub>–ERGO modified electrodes with high electrocatalytic performance for methanol oxidation†

A. T. Ezhil Vilian,<sup>a</sup> Shen-Ming Chen<sup>\*a</sup> and Shakkthivel Piraman<sup>b</sup>

We report on a process for the electrochemical synthesis of Pt particles on a composite of zirconium oxide/electrochemically reduced graphene oxide (ERGO) sheets. Zirconium oxide produces bridging molecules which allow easy anchoring of Pt particles to form a functional ERGO multilayer film produced through a co-electrochemical deposition procedure. The catalytic performance improves as a consequence of the addition of ZrO<sub>2</sub>, which increases the number of active Pt sites. Scanning electron microscopy (SEM), Raman spectrometry, X-ray diffraction (XRD), and electrochemical impedance spectroscopy (EIS) are used to characterize the microstructure and morphology of the fabricated Pt/ZrO<sub>2</sub>–ERGO electrode. It is found that this approach allows for the development of new kinds of electrocatalysts for use in direct methanol fuel cells. The process of methanol oxidation is investigated through cyclic voltammetry and amperometry. The results indicate that the Pt/ZrO<sub>2</sub>–ERGO electrocatalyst exhibits much higher catalytic activity and better stability than either the Pt/ERGO or commercially available Pt/C electrocatalysts as well as have better tolerance to CO during the electrooxidation of methanol. The Pt catalysts on the ZrO<sub>2</sub>–ERGO composite facilitate the methanol oxidation reaction making it a promising material for application in the direct methanol fuel cells that are used in the fields of biotechnology and environmental chemistry.

Received (in Porto Alegre, Brazil)  
31st August 2014,

Accepted 8th November 2014

DOI: 10.1039/c4nj01470g

www.rsc.org/njc

## 1. Introduction

Direct methanol fuel cells (DMFCs) are attracting increasing attention in both academia and industry as green power sources for vehicles and portable electronics, because they can convert chemical energy directly into electrical energy.<sup>1–3</sup> However, the commercial application of DMFCs is still hindered by the skyrocketing prices of scarce materials needed for their fabrication such as the Pt catalyst and the sluggish methanol oxidation reaction.<sup>4,5</sup> Therefore, substitutes for the carbon-based Pt catalysts are urgently needed, and improved Pt utilization and catalytic activity are the main issues for methanol fuel cell researchers.<sup>6</sup> A variety of strategies have been used to solve these problems, including optimizing the size and shape of the Pt nanoparticles, developing Pt nanoparticles with high energy facets

and alloying Pt with its neighboring transition metals such as Ru, Ni, Pd and Au. Pt nanoparticles have been used on different types of catalyst supports including carbon black, carbon nanotubes and mesoporous carbon.<sup>7,8</sup> Although different methods for the preparation of Pt based composites and the exhibited catalytic performance have been discussed in previous studies, a facile method for the preparation of Pt NPs with well-controlled dimensions and morphologies and effective loading remains a challenging task.<sup>9</sup>

Recently, the unique properties of graphene, which is a new kind of carbon material with a single layer of bonded-sp<sup>2</sup> carbons compacted into a two-dimensional honeycomb lattice, have attracted intense interest. Its extremely high surface area, excellent electrical conductivity and superior chemical stability make graphene a favorable candidate for electrocatalyst supports in DMFCs.<sup>10–12</sup> Graphene oxide (GO) has many oxygen-containing functional groups, such as hydroxyl, epoxide, carbonyl, and carboxyl groups, on its surface. These features give GO good solubility in aqueous solvents, even in some organic solvents, allowing the creation of more active sites for supporting metal oxides (*e.g.*, MnO<sub>2</sub>, TiO<sub>2</sub>, WO<sub>3</sub>, CeO<sub>2</sub>, and Fe<sub>2</sub>O<sub>3</sub>) which could have synergic effects to improve the performance of the catalysts.<sup>13–16</sup>

<sup>a</sup> Department of Chemical Engineering and Biotechnology, National Taipei University of Technology, No. 1, Section 3, Chung-Hsiao East Road, Taipei 106, Taiwan, Republic of China. E-mail: smchen78@ms15.hinet.net;

Fax: +886 2270 25238; Tel: +886 2270 17147

<sup>b</sup> Sustainable and Smart Materials Research Lab., Department of Nano Science and Technology, Alagappa University, Karaikudi 630 002, Tamil Nadu, India

† Electronic supplementary information (ESI) available. See DOI: 10.1039/c4nj01470g

Zirconium oxide (ZrO<sub>2</sub>) nanomaterials are also industrially important because of their unique combination of properties like thermal stability, chemical inertness, and lack of toxicity.<sup>17–19</sup> In the present study, we investigated ZrO<sub>2</sub> nanostructures as an excellent candidate material for use in various applications, such as fuel cells, optical coatings, flat panel displays with low-energy excitation sources, solar energy converters, optical amplifiers, photonic devices, and so on.<sup>20–23</sup>

To the best of our knowledge, there have been no studies on the use of platinum particle decorated ZrO<sub>2</sub>-ERGO composites as supports for high electron and proton conductivity. To fill this gap, this study investigates the electrochemical behavior and electrocatalytic activity of a Pt/ZrO<sub>2</sub>-ERGO electrode for methanol oxidation. It is found that the electrochemically active surface area of Pt/ZrO<sub>2</sub>-ERGO is higher than observed for the Pt/ERGO or commercially available Pt/C electrocatalysts. The Pt/ZrO<sub>2</sub>-ERGO modified electrode has higher electrocatalytic activity, leading to better performance and should be suitable for application in highly stable methanol fuel cells. In this study, a Pt/ZrO<sub>2</sub>-ERGO modified electrode is used as the anode and Nafion 112 as the membrane. During subsequent testing of the direct methanol fuel cell it was found to have a maximum power density of 125 mW cm<sup>-2</sup> at 30 °C.

## 2. Experimental procedure

### 2.1 Chemicals

Graphite powder (<20 μm), zirconyl chloride octahydrate (ZrOCl<sub>2</sub>), potassium hexachloroplatinate(IV), Nafion 112, and commercial Pt/C were purchased from Sigma-Aldrich while perchloric acid (HClO<sub>4</sub>) and methanol were purchased from Wako Chemicals. All other chemicals were of analytical grade. Deionized water was obtained from a Millipore Milli-Q purification system (18.2 MΩ cm).

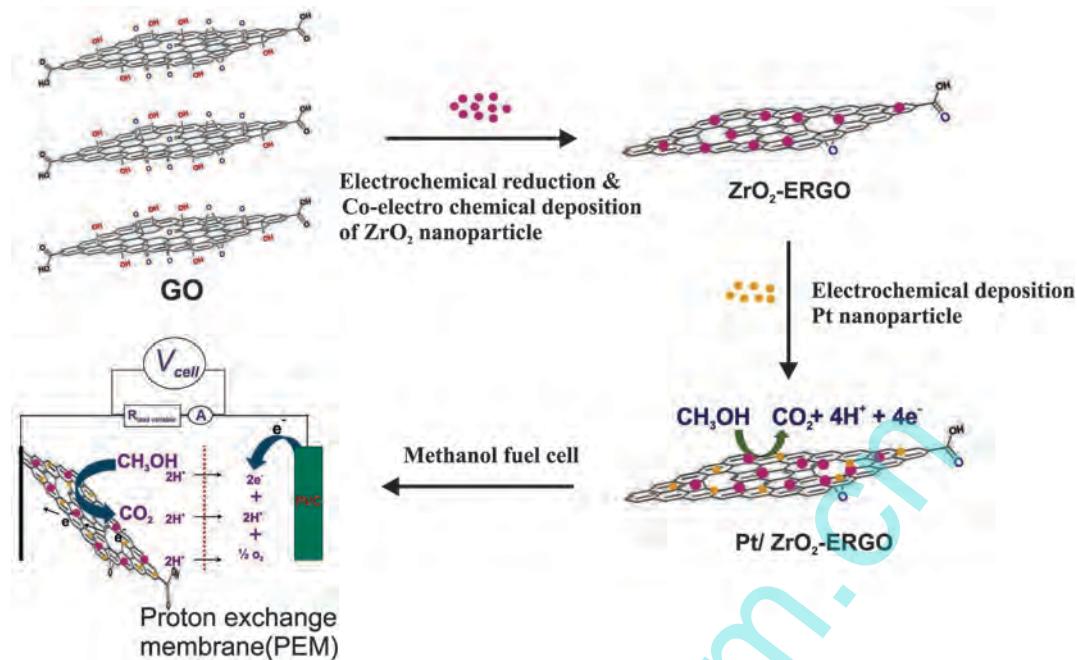
### 2.2 Apparatus

The electrochemical activity of the electrocatalysts was evaluated by cyclic voltammetry (CV) using a three-electrode system and a CHI 405A model electrochemical workstation. The Pt/ZrO<sub>2</sub>-ERGO working electrode was an electrocatalyst modified GCE (geometric area = 0.07 cm<sup>2</sup>). A saturated Ag/AgCl (sat. KCl) electrode was used as the reference electrode and a platinum wire electrode served as the counter electrode. Electrochemical impedance spectroscopic measurements of the samples were performed (using an EIM6ex ZAHNER, Kroanach, Germany) in the frequency range of 0.1 Hz to 100 kHz. Scanning electron microscopy (SEM) was performed on the prepared composite using a Hitachi S-3000 H scanning electron microscope. Energy-dispersive X-ray spectroscopy (EDX) was carried out for the composite films using a HORIBA EMAX X-ACT Model 51-ADD0009. The atomic force microscopic (AFM) images were collected using a multimode scanning probe microscope (Being Nano-Instruments CSPM-4000, China), the transmission electron microscopic (TEM) images were recorded using a Philips TECNAI 20 microscope (200 kV) and the Fourier-transform infrared (FTIR) spectra were obtained using a Perkin

Elmer RXI spectrometer. The Raman spectra were recorded using a Raman spectrometer (RENISHAW inVia system, UK) using a 514.4 nm He/Ne laser. The as-prepared composite films were coated onto the ITO and then dried overnight prior to X-ray diffraction (XRD) analysis. The crystal structures of the product were characterized by the X-ray diffraction system (PANalytical B.V., The Netherlands) using Cu Kα as the radiation source at an operating voltage of 40 kV and a scan rate of 60 min<sup>-1</sup>. The current and power were measured using precision multimeters (Keithley Instruments; model 2400) in a room temperature atmosphere.

### 2.3 Preparation of electrocatalysts

GO was synthesized from natural graphite powder (99.9%) using the well-known modified Hummer's method.<sup>24</sup> Briefly, 1 g of graphite was suspended in 2.5 g of K<sub>2</sub>S<sub>2</sub>O<sub>8</sub>, after which 46 ml of H<sub>2</sub>SO<sub>4</sub> was added followed by stirring in an ice-bath. Next, 2.5 g of P<sub>2</sub>O<sub>5</sub> was added gradually during stirring and cooling, maintaining the temperature of the mixture below 20 °C. Then 6 g of KMnO<sub>4</sub> and 1 g of NaNO<sub>3</sub> were slowly added to the beaker while the temperature was maintained below 20 °C. The reaction was terminated by adding 250 ml of deionized water followed by 6 ml of H<sub>2</sub>O<sub>2</sub> (30 wt%). The solid suspension was filtered, washed with a 2 M HCl solution and then 3–4 times in ethanol and dried in a vacuum at 60 °C overnight. Then, graphene oxide (1 g) was exfoliated in deionized water (1 mL) during ultrasonic treatment for 1 hour to form a light-brown solution. Before modification, the bare glassy carbon electrode (GCE) with a diameter of 3 mm was polished with an alumina (particle size of about 0.05 μm)/water slurry using a Buehler polishing kit and washed ultrasonically in double distilled water before being dried. Then 5 μL of the as-prepared GO suspension were dropped onto the surface of the pretreated GCE electrode and dried. Then the GO modified electrode was transferred into a 0.05 M phosphate buffer solution comprised of 5.0 mM ZrOCl<sub>2</sub> in PBS (pH 5). After this, 10 consecutive cyclic voltammograms were recorded at a potential ranging from 0 to -1.5 V at a scan rate of 20 mV s<sup>-1</sup> (see Fig. S1B, ESI†). After this, ZrO<sub>2</sub>-ERGO/GCE was moved to an electrochemical cell containing 1 mM K<sub>2</sub>PtCl<sub>6</sub> in a 0.5 M H<sub>2</sub>SO<sub>4</sub> solution then recorded for 10 cycles at a potential range from -0.25 to 1.0 V (see Fig. S1C, ESI†). The Pt/ZrO<sub>2</sub>-ERGO modified electrode was rinsed with double distilled water and dried using N<sub>2</sub>. The CV measurements were carried out at a potential ranging from -0.2 to 1.0 V at a scan rate of 50 mV s<sup>-1</sup> in both 1 M HClO<sub>4</sub> electrolyte solution and 1 M HClO<sub>4</sub> + 1 M CH<sub>3</sub>OH electrolyte solution. A simple methanol fuel cell was constructed using the Pt/ZrO<sub>2</sub>-ERGO modified GCE as an anode and the commercially available Pt/C as a cathode. Nafion 112 was used as the membrane in our homemade fuel cell setup in our laboratory. Using a 1 M concentration methanol solution, the direct methanol fuel cell is reported to exhibit higher open circuit voltages and power density output. The synthesis and fabrication of Pt/ZrO<sub>2</sub>-ERGO electrocatalysts are illustrated in Scheme 1. Polarization and power curves were recorded in a 1 M methanol aqueous solution.



Scheme 1 Schematic representation of methanol oxidation taking place at the Pt/ZrO<sub>2</sub>-ERGO electrocatalyst modified electrode.

### 3. Results and discussion

#### 3.1 Surface and composite analysis

Fig. 1 shows some typical SEM images obtained for the ERGO/ITO, Pt/ERGO/ITO, and Pt/ZrO<sub>2</sub>-ERGO/ITO electrodes. Fig. 1A displays an SEM image of ERGO and the corresponding EDX elemental analysis. One can see the typical ERGO flakes with broad lamellar structures or folds, which provide the larger surface-area. In addition, the EDX elemental analysis of ERGO shows the presence of C (85%) and O (15%) as can be seen in Fig. 1D. The results clearly indicate that the electrochemical reduction has been effective. The oxygen functionalities and negative charges at the ERGO surface favor the adsorption of ZrO<sub>2</sub>.

Further removal of these oxygen-containing groups leads to a remarkable increase in the ZrO<sub>2</sub> particle size due to aggregation. The oxygen-containing groups on the ERGO surface play an important role in enhancing the loading of ZrO<sub>2</sub>. The SEM image in Fig. 1C displays small granular shaped ZrO<sub>2</sub> particles that have been deposited on the ERGO surface which provide a large surface area for the incorporation of the spherically shaped Pt particles. The Pt particles were well distributed on the surface of ZrO<sub>2</sub>-ERGO to form the Pt/ZrO<sub>2</sub>-ERGO/ITO composite film. Furthermore, the composition of this Pt/ZrO<sub>2</sub>-ERGO/ITO composite film was also confirmed by EDX spectroscopy (Fig. 1F) to be comprised of C (12%), O (66%), Zr (22%), and Pt (22%).

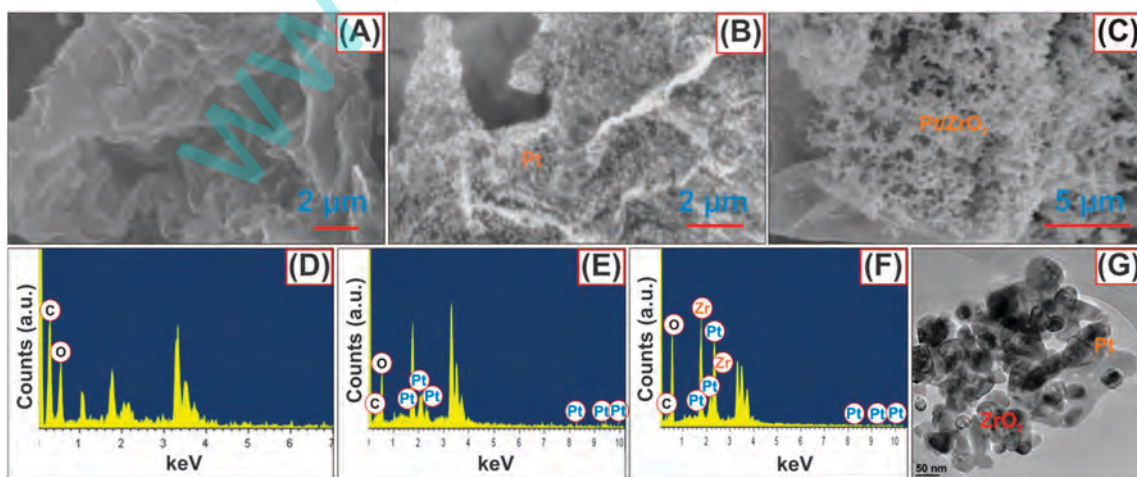


Fig. 1 SEM images of the (A) ERGO/ITO, (B) Pt/ERGO/ITO, (C) Pt/ZrO<sub>2</sub>-ERGO/ITO modified films, and EDX spectra of (D) ERGO/ITO, (E) Pt/ERGO/ITO, and (F) ZrO<sub>2</sub>-ERGO/ITO and the HRTEM image of the (G) Pt/ZrO<sub>2</sub>-ERGO modified film.

All of the results suggest that  $\text{ZrO}_2$ -ERGO was well covered by Pt particles. The morphology of the as-prepared composite was further confirmed using HRTEM. Fig. 1G shows a HRTEM image of the Pt/ $\text{ZrO}_2$ -ERGO electrocatalyst. The Pt nanoparticles are spherical in shape while the  $\text{ZrO}_2$  particles have grown into larger grains. The granular surface microstructures on the particles also disappeared upon reducing the porosity of the surface. The uniform distribution on the ERGO sheet is also shown. There is some corrugation and scrolling at the edges of the ERGO, but it can be clearly seen that the ERGO sheet is decorated with uniformly distributed spherical Pt/ $\text{ZrO}_2$  nanoparticles. Fig. 1G shows the Pt/ $\text{ZrO}_2$  nanoparticles anchored on the surface of both sides of the ERGO sheets. The good dispersion behavior and larger surface area, which provided more active sites and electrocatalytic reaction centers, make this a potential material for use in an electrochemical sensor.

### 3.2 Characteristics of the Pt/ $\text{ZrO}_2$ -ERGO composite

Fig. 2A presents the FT-IR spectra of (a) GO and (b) Pt/ $\text{ZrO}_2$ -ERGO. The GO spectrum is in good agreement with that observed in previous work.<sup>25</sup> GO is a two-dimensional carbon sheet in which there exists a large amount of oxygen functional groups such as hydroxyl, carboxyl and epoxide groups. The broad peak of GO in Fig. 2A(a) at  $3444.5\text{ cm}^{-1}$  can be ascribed to the stretching

of O-H.<sup>26</sup> After reduction, as can be seen in ERGO (Fig. S3(a), ESI<sup>†</sup>), the most intense peak at  $1165\text{ cm}^{-1}$  displays the presence of C-O stretching vibration, and the second most intense peak at  $1545\text{ cm}^{-1}$  corresponds to the C=C stretching of the skeletal in-plane vibration. The peaks in the range  $2920\text{ cm}^{-1}$  to  $2850\text{ cm}^{-1}$  correspond to the asymmetric C-H stretching; in addition, a small peak positioned at  $1736\text{ cm}^{-1}$  can be attributed to the stretching vibration of C=O. Fig. S3 (ESI<sup>†</sup>) presents the FT-IR spectra of (b) the  $\text{ZrO}_2$ -ERGO nanocomposite, the intensity of the peak at  $1557\text{ cm}^{-1}$  gets maximized, which is due to the skeletal in-plane vibration of C=C, whereas it is less pronounced in RGO data. The formation of ERGO was confirmed by the decrease of intensity or even suppression of different oxygen functionalities, which clearly leads to a further reduction of GO to RGO. On the other hand, there is a significant decrease in the intensity of these peaks in the FT-IR spectra of the Pt/ $\text{ZrO}_2$ -ERGO film, with some of them vanishing completely. This indicates that the bulk of the oxygen-containing functional groups was removed from GO. A new peak can be observed at about  $1560\text{ cm}^{-1}$  in the Pt/ $\text{ZrO}_2$ -ERGO spectra, which can be attributed to the skeletal vibration of the graphene sheets.

The Raman spectra of GO,  $\text{ZrO}_2$ -ERGO and Pt/ $\text{ZrO}_2$ -ERGO are shown in Fig. 2B. For all three samples we observe two bands, which correspond (the D band and the G band) to the Raman spectrum of GO,  $\text{ZrO}_2$ -ERGO and Pt/ $\text{ZrO}_2$ -ERGO located

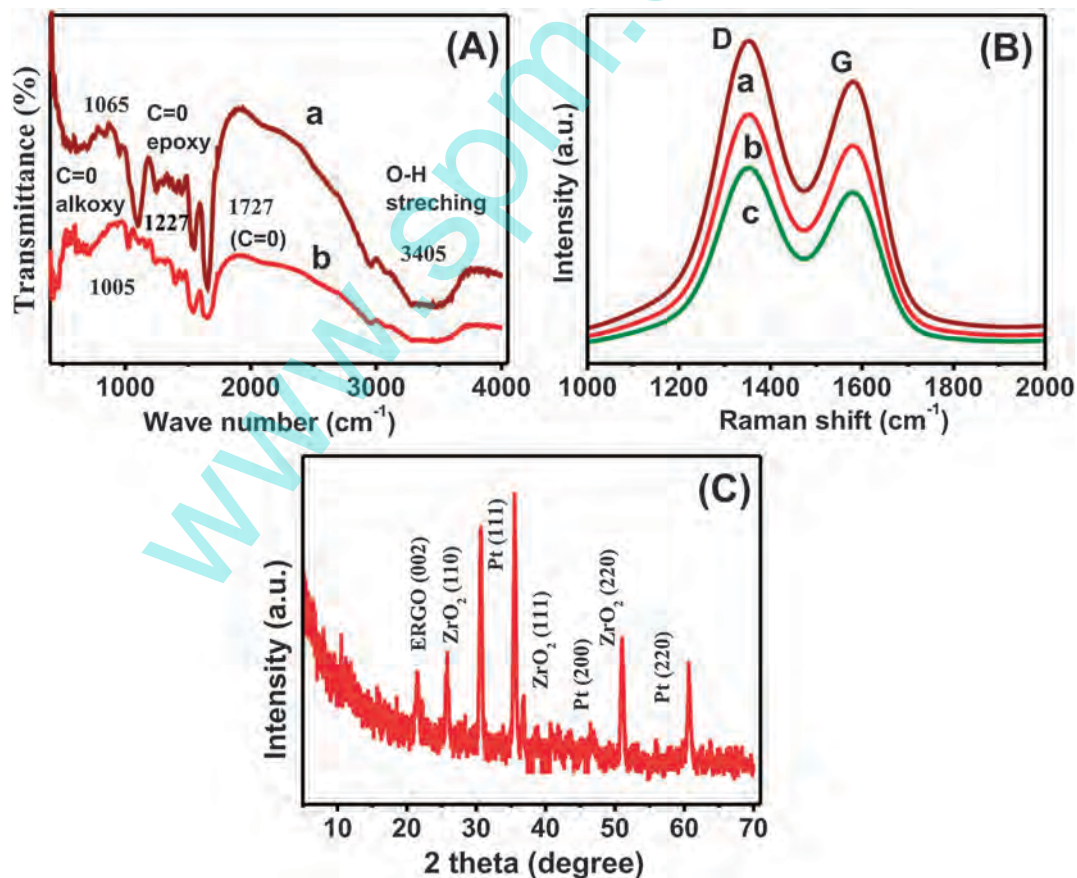


Fig. 2 (A) FTIR spectra of (a) GO and (b) the Pt/ $\text{ZrO}_2$ -ERGO composite, (B) Raman spectra of (a) GO, (b)  $\text{ZrO}_2$ -ERGO and (c) the Pt/ $\text{ZrO}_2$ -ERGO composite, and XRD analysis results of the Pt/ $\text{ZrO}_2$ -ERGO/ITO modified film.

at 1352 and 1585  $\text{cm}^{-1}$  respectively. The intensity ratio of the D band to the G band ( $I_D/I_G$ ) for Pt/ZrO<sub>2</sub>-ERGO correlates with the average size of the sp<sup>2</sup> domains, that is, the smaller the size of the sp<sup>2</sup> domains, the higher the  $I_D/I_G$  intensity ratio. From Fig. 2B, we can say that the intensity ratio of D and G bands ( $I_D/I_G$ ) of the GO (1.09) sample is obviously larger than that of ZrO<sub>2</sub>-ERGO (1.16) which confirms that most of the oxygenated groups would have been removed during the electrochemical reduction process or which is regarded as the successful modification of ZrO<sub>2</sub> on the ERGO sheets. On the other hand, the  $I_D/I_G$  ratio varies from 1.09 for GO to 1.38 for the Pt/ZrO<sub>2</sub>-ERGO composites.<sup>27,28</sup> The D to G band intensity ratio ( $I_D/I_G$ ) is generally expected to reflect the defect density of the carbonaceous material, which is more concentrated in Pt/ZrO<sub>2</sub>-ERGO than in GO. It can be concluded that Pt/ZrO<sub>2</sub>-ERGO showed the few-layer feature of graphene. Thus, the Raman results are consistent with the HRTEM characterization, clearly showing the few-layer feature of graphene.

Fig. 2C shows the XRD patterns of Pt/ZrO<sub>2</sub>-ERGO. A broad and weak (002) diffraction peak arising from the slight stacking of the graphene sheets is also detected at a  $2\theta$  of about 25°, confirming the successful reduction of GO into ERGO. The XRD patterns of the ZrO<sub>2</sub> particles in Fig. 2C show diffraction peaks at  $2\theta = 30^\circ$  (110),  $38^\circ$  (111) and  $52^\circ$  (220) which are characteristic of the ZrO<sub>2</sub> particle structure, and indicative of the formation of ZrO<sub>2</sub> particles on ERGO.<sup>29</sup> The peaks between 30° and 90° can be indexed to Pt crystals with a face-centered cubic (fcc) structure. The peaks at  $2\theta = 39.7^\circ$ ,  $46.3^\circ$ , and  $67.6^\circ$  are assigned to the (111), (200), and (220) planes of the Pt particles (according to the standard card for cubic Pt, JCPDS No. 04-0802). This indicates that alloying has occurred, caused by the incorporation of the smaller ZrO<sub>2</sub> particles into the Pt fcc structure.<sup>30,31</sup> The average size of the Pt particles electrodeposited on ZrO<sub>2</sub>-ERGO was calculated using Scherrer's eqn (1):

$$d = \frac{0.9\lambda}{\beta \cos\theta_B}, \quad (1)$$

where  $d$  is the diameter (Å);  $\lambda$  is the wavelength of the X-ray radiation (1.54056 Å);  $\beta$  is the full-width half-maximum of the respective diffraction peaks; and  $\theta_B$  is the angle at the peak maximum. The calculated average particle size of Pt particles on ZrO<sub>2</sub>-ERGO is about 20 nm. This result is in good agreement with the AFM results. However, the AFM results reveal the Pt particles to have a spherical morphology (Fig. S2C, ESI†). From the histogram of the size distribution, the average size of the Pt particles was found to center at around 20 nm (Fig. S2D, ESI†). The XRD results also indicate that Pt particles were obtained on the ZrO<sub>2</sub>-ERGO sheets. The EDX measurements verify the existence of Pt on the ZrO<sub>2</sub>-ERGO surface.

### 3.3 Electrochemical performance of the fabricated modified electrodes

Fig. 3A shows the representative cyclic voltammetry (CV) curves of (a) Pt/C, (b) Pt/ZrO<sub>2</sub>, (c) Pt/ERGO, and (d) Pt/ZrO<sub>2</sub>-ERGO electrocatalysts in a 1 M HClO<sub>4</sub> solution. The scan rate was 50 mV s<sup>-1</sup> between -0.2 V and 1.0 V, as shown in Fig. 3A.

For comparison, the cyclic voltammograms of the Pt/C (34.02 m<sup>2</sup> g<sup>-1</sup>), Pt/ZrO<sub>2</sub> (36.13 m<sup>2</sup> g<sup>-1</sup>), Pt/ERGO (42.93 m<sup>2</sup> g<sup>-1</sup>) and Pt/ZrO<sub>2</sub>-ERGO (68.2 m<sup>2</sup> g<sup>-1</sup>) electrocatalysts are also shown. For the Pt/C, Pt/ZrO<sub>2</sub> electrocatalyst, a poorly resolved peak is observed in the hydrogen adsorption/desorption region. The electrochemically active surface area (EAS) (m<sup>2</sup> g<sup>-1</sup> Pt) of Pt deposited on the surface of different modified electrodes is calculated according to the charge in hydrogen desorption ( $Q_H$ , mC cm<sup>-2</sup>) as follows:<sup>32</sup>

$$\text{EAS} = Q_H/0.21W_{\text{Pt}}, \quad (2)$$

where  $W_{\text{Pt}}$  is the Pt loading (g cm<sup>-2</sup>) on the surface of different modified electrodes and 0.21 is the charge (mC cm<sup>-2</sup>) required to oxidize a monolayer of adsorbed hydrogen atoms on the platinum surface. The Pt/ZrO<sub>2</sub>-ERGO electrocatalyst exhibits a relatively broader peak with a slightly higher current in the adsorption/desorption region compared to the Pt/ERGO electrocatalyst. It can be seen that Pt particles may originate from the more uniformly covered surface of the ZrO<sub>2</sub>-ERGO composites. The smaller particles would be responsible for their good electrochemical catalytic performance. The results of the investigation of the activity of the Pt/ZrO<sub>2</sub>-ERGO electrocatalyst described in our work show well-defined hydrogen adsorption/desorption peaks with a much larger area in the potential region of -0.2 V to 1.0 V, demonstrating the higher surface area of the electrocatalyst. The greater surface area may be owed to the high deposition rate and small size of the Pt particles on the ZrO<sub>2</sub>-ERGO composites. Furthermore, ZrO<sub>2</sub> increased the concentration of the OH<sub>ads</sub> species on the electrocatalyst surface, and these OH<sub>ads</sub> species then reacted with CO-like intermediate species to produce CO<sub>2</sub> products, releasing the active sites on Pt for further electrochemical reaction. The formation of Pt adsorbed carbonaceous intermediates (mainly CO) occurs during the methanol oxidation at the Pt/ZrO<sub>2</sub>-ERGO electrocatalysts is illustrated by the following mechanism:<sup>33</sup>

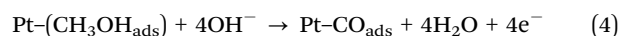
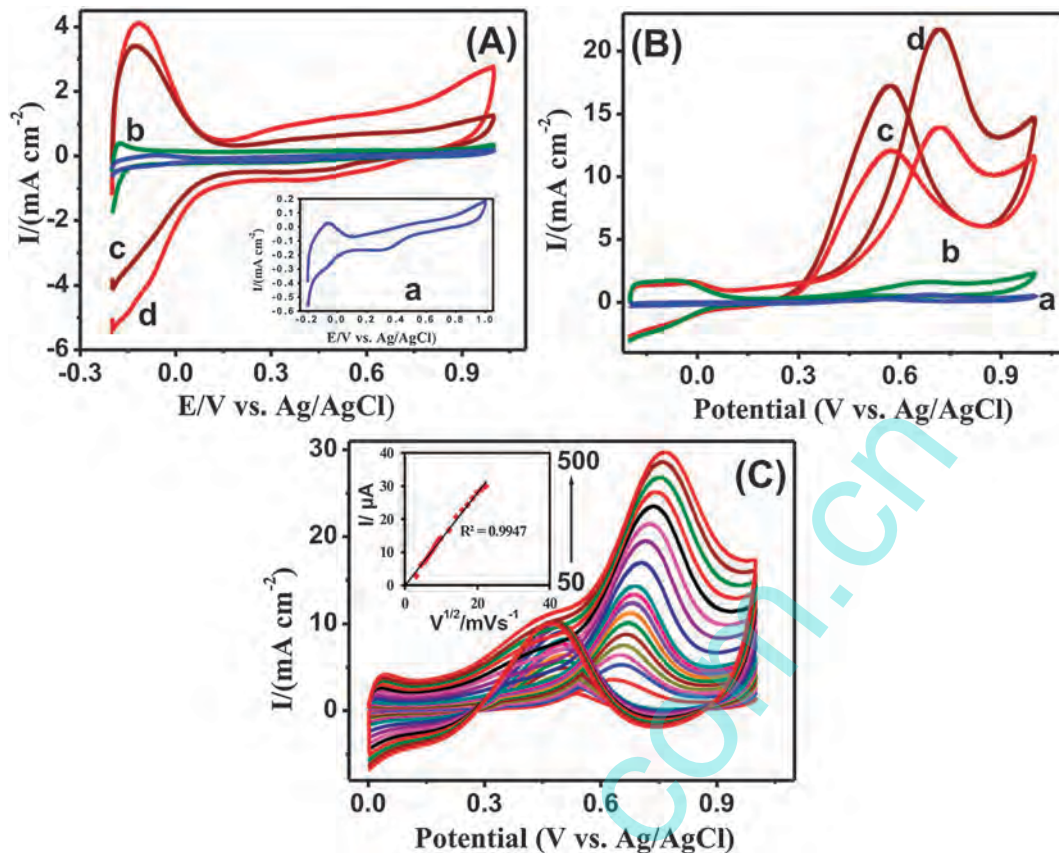


Fig. 3B shows the typical cyclic voltammograms of methanol oxidation for catalysis in a 1 M HClO<sub>4</sub> solution, at a scan rate of 50 mV s<sup>-1</sup> between -0.2 V and 1.0 V by the: (a) Pt/C, (b) Pt/ZrO<sub>2</sub>, (c) Pt/ERGO, and (d) Pt/ZrO<sub>2</sub>-ERGO electrodes. The peak current of the maximum current density of the forward peak ( $I_f$ ) is related to the oxidation of freshly chemisorbed species released from methanol adsorption, and that of the backward peak ( $I_b$ ) represents the removal of carbonaceous species incompletely oxidized in the forward scan. The ratio of the maximum current to the peak anodic current ( $I_f/I_b$ ) in the forward sweep to the reverse sweep is utilized in order to assess the electrocatalyst's tolerance for the accumulation of intermediate species. The  $I_f/I_b$  ratio can be used to describe the CO tolerance of an electrocatalyst for comparison with the accumulation of carbonaceous species such as CO on the electrode surface. A lower ratio of the forward anodic peak current density ( $I_f$ ) to the reverse anodic peak current density ( $I_b$ ) indicates poor oxidation of methanol



**Fig. 3** (A) CV curves of the (a) Pt/C, (b) Pt/ZrO<sub>2</sub>, (c) Pt/ERGO and (d) Pt/ZrO<sub>2</sub>-ERGO modified electrodes in 1 M HClO<sub>4</sub> without methanol (scan rate = 50 mV s<sup>-1</sup>). (B) Cyclic voltammograms of the (a) Pt/C, (b) Pt/ZrO<sub>2</sub>, (c) Pt/ERGO and (d) Pt/ZrO<sub>2</sub>-ERGO modified electrodes in 1 M HClO<sub>4</sub> with 1 M CH<sub>3</sub>OH (scan rate = 50 mV s<sup>-1</sup>). (C) Cyclic voltammograms of Pt/ZrO<sub>2</sub>-ERGO in 1 M HClO<sub>4</sub> with 1 M CH<sub>3</sub>OH aqueous solutions at different scan rates (10–100 mV s<sup>-1</sup>). Inset: the relationship between the peak currents and the square root of the scan rates.

as opposed to CO<sub>2</sub> during the forward anodic scan with excessive accumulation of carbonaceous residues on the electrocatalyst surface. Remarkably, a higher  $I_p/I_b$  value suggests that the electrocatalysts are more efficient in lowering the adsorbed carbon monoxide. The value is a useful way of comparing the long-term catalytic activity between different electrocatalysts. As shown in Fig. 3B, the  $I_p/I_b$  ratio of the (d) Pt/ZrO<sub>2</sub>-ERGO electrocatalyst is 1.92; (c) the  $I_p/I_b$  value of Pt/ERGO is 1.12; and (b) the  $I_p/I_b$  value of Pt/ZrO<sub>2</sub> is 1.02, which are substantially higher than that of 0.98 of (a) the  $I_p/I_b$  value of Pt/C (see Table 1). The results show the better catalytic tolerance of these composites, and indicate lower accumulation of CO-like species on the electrocatalyst during the methanol oxidation reaction, thus leading to excellent catalytic activity.

**Table 1** Electrochemical properties of different electrocatalysts

Electrocatalyst	Onset potential (V)	EAS (m <sup>2</sup> g <sup>-1</sup> )	$I_p/I_b$	$I^a$ (mA)	Normalized current <sup>b</sup> (%)
Pt/ZrO <sub>2</sub> -ERGO	0.335	68.2	1.92	6.12	92
Pt/ERGO	0.406	42.93	1.12	3.88	66
Pt/ZrO <sub>2</sub>	0.491	36.13	1.02	1.2	42
Pt/C	0.535	34.02	0.98	0.5	36

<sup>a</sup>  $I$  is the residual current at 0.65 V after 1500 s. <sup>b</sup> Normalized current (%) is the percentage of the peak current of the 200th cycle compared to the maximum peak current.

A summary of the different modified electrodes and their  $I_p/I_b$  values is given in Table 2. The higher electrochemical performance observed here can probably be attributed to the higher utilization of Pt on ZrO<sub>2</sub>-ERGO. The greater surface area provided leads to higher electrocatalytic activity, most likely due to the large number of nucleation centers available on the surface of ERGO. The unique structure of the support appears to enable Pt on ZrO<sub>2</sub>-ERGO to have higher specific activity leading to the higher methanol oxidation performance. This represents a class of functional electrocatalysts with promising properties for DMFCs.

Further investigation was done to explore the transport characteristics and electrocatalytic oxidation of methanol on the Pt/ZrO<sub>2</sub>-ERGO electrodes in the 1 M HClO<sub>4</sub> + 1 M CH<sub>3</sub>OH aqueous solutions at different sweep rates. Fig. 3C shows the dependence curve of the peak currents for the square root of the scan rates. The peak currents are linearly proportional to the square root of the scan rates. In addition,  $E_p$  moves to slightly higher potentials with an increasing scan rate, which suggests that the electrocatalytic oxidation of methanol on Pt/ZrO<sub>2</sub>-ERGO electrodes is a diffusion-controlled process.<sup>34</sup>

### 3.4 Chronoamperometric studies

Chronoamperometry is an effective method for investigating the long-term stability and performance of different electrocatalysts

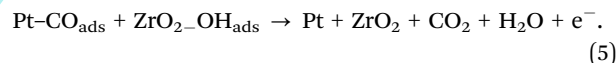
Table 2 Comparison of the performance of the proposed Pt/ZrO<sub>2</sub>-ERGO electrocatalysts with other electrocatalysts<sup>a</sup>

Samples	Onset potential (V)	EAS (m <sup>2</sup> g <sup>-1</sup> )	I <sub>f</sub> /I <sub>b</sub>	Ref.
Pt/ZrO <sub>2</sub> -ERGO	0.480	68.2	1.92	This work
Pt-Ru-graphite	0.500	—	1.52	35
Pt/MWCNT	0.300	33.43	0.72	36
Pt-reduced graphene oxide-supported WC nanocrystallites	0.250	253.12	1.26	37
Pt/graphene nanosheets-β-cyclodextrin	0.350	36.20	1.32	38
Pt 7% CeO <sub>2</sub> /graphene	0.659	66.4	1.48	39

<sup>a</sup> I<sub>f</sub>/I<sub>b</sub> represents the ratio between the forward and backward anodic peak currents.

(Pt/C, Pt/ZrO<sub>2</sub>, Pt/ERGO and Pt/ZrO<sub>2</sub>-ERGO) and is used for samples immersed in 1 M HClO<sub>4</sub> and 1 M CH<sub>3</sub>OH at 0.65 V for 3200 seconds. As can be seen in Fig. 4A, the current density of Pt/ZrO<sub>2</sub>-ERGO remains higher than that of the other electrocatalysts on the Pt/C, Pt/ZrO<sub>2</sub>, Pt/ERGO, Pt/ZrO<sub>2</sub>-ERGO modified electrodes throughout the whole test range. The results indicate that the former is more active than the latter in relation to methanol oxidation. There is a slight current decay due to the unavoidable formation of Pt adsorbed reaction intermediates during methanol oxidation and enhanced electrocatalytic activity. Table 1 shows the electrochemical properties of Pt/C, Pt/ZrO<sub>2</sub>,

Pt/ERGO and Pt/ZrO<sub>2</sub>-ERGO. The current density at 1500 s is 6.12 mA mg<sup>-1</sup> for Pt/ZrO<sub>2</sub>-ERGO, much higher than that observed for Pt/ERGO (3.88 mA mg<sup>-1</sup>), Pt/ZrO<sub>2</sub> (1.2 mA mg<sup>-1</sup>) and Pt/C (0.5 mA mg<sup>-1</sup>). Pt/ZrO<sub>2</sub>-ERGO has the best stability during methanol oxidation out of all the electrocatalysts. It should be noted that the current decay is slower for Pt/ZrO<sub>2</sub>-ERGO than for Pt/ERGO, indicating that the incorporation of Pt into ZrO<sub>2</sub>-ERGO reduces the poisonous effect and enhances the catalytic stability during methanol oxidation. The process can be summarized as follows. Firstly, ZrO<sub>2</sub> offers more active sites for the improved deposition of Pt particles, which results in a larger active surface area on the Pt/ZrO<sub>2</sub>-ERGO electrocatalysts. Secondly, the hydroxyl groups adsorbed onto the ZrO<sub>2</sub> surface may act to remove the adsorbed carbonyl groups from the surface of Pt, allowing the dissociation-adsorption of methanol to proceed more quickly. In addition, the Pt particles on the surface of the ZrO<sub>2</sub>-ERGO electrocatalysts may act as active centers during the process of methanol oxidation. The surface reaction of CO with OH probably takes place in the following form (5):



By this means the CO-poisoned Pt/ZrO<sub>2</sub>-ERGO electrocatalysts can be regenerated, thereby partially eliminating the CO poisoning effect.

### 3.5 Electrochemical impedance spectroscopy (EIS) studies

Fig. 4B shows the EIS spectra and Nyquist plots (*Z'* versus “-*Z''*”) of the (a) Pt/C, (b) Pt/ERGO, (c) Pt/ZrO<sub>2</sub> and (d) Pt/ZrO<sub>2</sub>-ERGO/GCE electrodes in 1 M HClO<sub>4</sub> + 1 M CH<sub>3</sub>OH aqueous solutions at a potential of 0.5 V, for comparison EIS spectra of the saturated Ag/AgCl electrode, and the corresponding Nyquist plots are also shown. Obviously, significant differences in the impedance spectra are observed for different electrodes. Fig. 4B illustrates the Nyquist diagrams for the large charge transfer resistance *R*<sub>ct</sub> of 948 Ω for Pt/ERGO/GCE which can be attributed to the high C/O ratio making the molecules less electrically conductive and adding an additional increased electron transfer resistance for GCE. A further decrease in the *R*<sub>ct</sub> value to 448 Ω was observed after the deposition of Pt/ZrO<sub>2</sub> nanoparticles on the GCE surface (Fig. 4B, curve c). The results confirm that the *R*<sub>ct</sub> value of the Pt/ERGO modified electrode is larger than that of the Pt/ZrO<sub>2</sub> modified electrode. After the assembly of the Pt particles on the ZrO<sub>2</sub>-ERGO layer, there was a dramatic decrease in the semi-circular diameter of 208.4 Ω (a), attributable to Pt obstructing

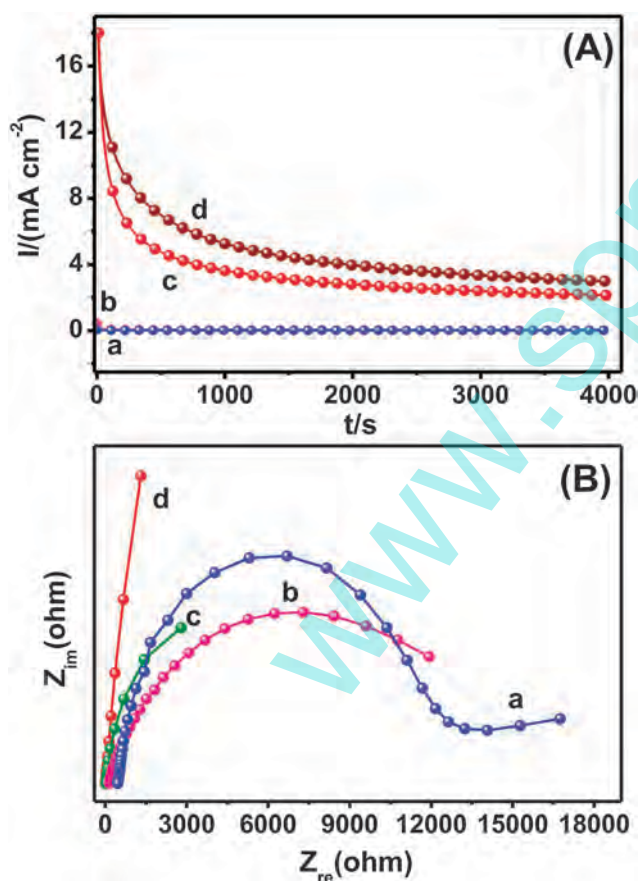


Fig. 4 (A) Chronoamperograms of the (a) Pt/C, (b) Pt/ZrO<sub>2</sub>, (c) Pt/ERGO, and (d) Pt/ZrO<sub>2</sub>-ERGO electrodes at 0.65 V in 1 M HClO<sub>4</sub> + 1 M CH<sub>3</sub>OH aqueous solutions. (B) EIS spectra of the (a) Pt/C, (b) Pt/ERGO/GCE, (c) Pt/ZrO<sub>2</sub>/GCE and (d) Pt/ZrO<sub>2</sub>-ERGO/GCE electrodes in 1 M HClO<sub>4</sub> + 1 M CH<sub>3</sub>OH aqueous solutions at 0.5 V. Frequency range: 0.1 Hz to 100 kHz. Inset: Randles equivalence circuit.

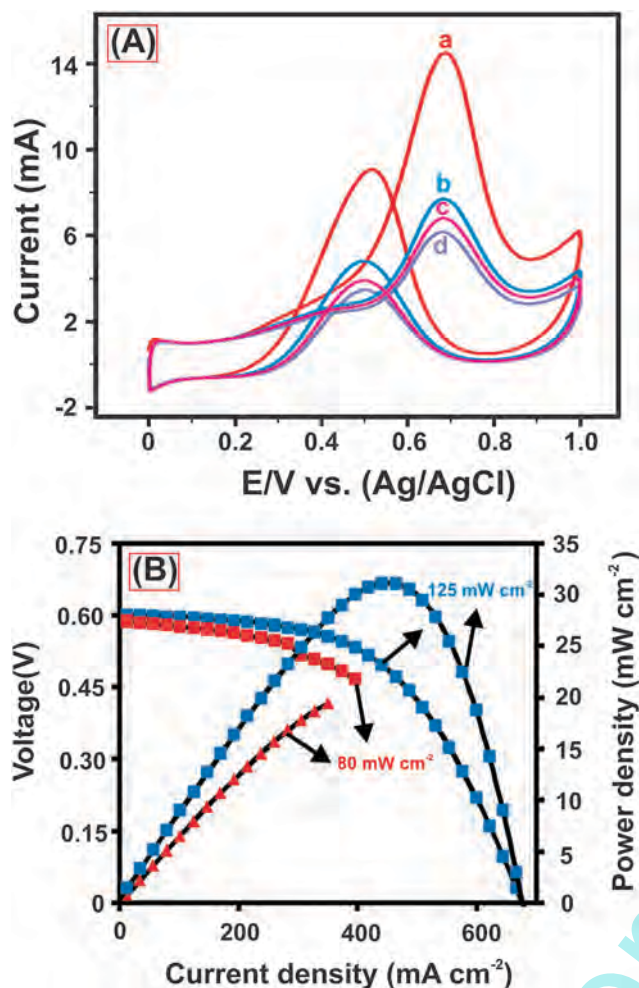


Fig. 5 (A) Cyclic voltammograms of Pt/ZrO<sub>2</sub>-ERGO with 1 cycle (a), 50 cycles (b), 100 cycles (c), and 200 cycles (d) in a nitrogen saturated solution of 1 M HClO<sub>4</sub> containing 1 M CH<sub>3</sub>OH at a scan rate of 50 mV s<sup>-1</sup>. (B) Cell polarization and power density curves obtained using the Pt/ZrO<sub>2</sub>-ERGO catalyzed anode and a Pt/C black catalyzed cathode in 1 M HClO<sub>4</sub> + 1 M CH<sub>3</sub>OH electrolyte aqueous solutions; Nafion 112; cell temperature 30 °C.

the electron transfer tunneling and higher electrocatalytic activity leading towards methanol electrooxidation. Pt/ZrO<sub>2</sub>-ERGO has a low C/O ratio. There was a remarkable decrease in the  $R_{et}$  value of Pt/ZrO<sub>2</sub>-ERGO after the Pt particles grew on ZrO<sub>2</sub>-ERGO/GCE. It can be seen that the semicircular diameter of the Pt/C modified electrode is much larger than that of the Pt/ZrO<sub>2</sub>-ERGO electrode. This suggests that the Pt/ZrO<sub>2</sub>-ERGO composite film has higher stability as an electrocatalyst. In other words, this result indicates higher electrocatalytic activity towards methanol oxidation.

It is well known that the long-term cyclic stability of electrocatalysts is necessary for practical applications. The long-term stability of Pt/ZrO<sub>2</sub>-ERGO electrocatalysts was investigated by using the cyclic voltammetric method after immersion in a 1 M HClO<sub>4</sub> + 1 M CH<sub>3</sub>OH solution for 200 cycles. The results are presented in Fig. 5A. It can be seen that the peak current decreased gradually with successive scans. By the 200th scan the peak current was about 92% of that of the first scan. The loss of the

peak current during methanol oxidation may be the result of the consumption of methanol over the long time it took for the cyclic voltammetry scans. The Pt/ZrO<sub>2</sub>-ERGO electrocatalysts exhibit excellent long-term cycle stability, which further suggests that they are favorable candidates for use in DMFCs (see Fig. S4, ESI<sup>†</sup>). The Pt/ZrO<sub>2</sub>-ERGO electrocatalysts shows higher stability than that of (a) Pt/C (36%), (b) Pt/ZrO<sub>2</sub> (42%), and (c) Pt/ERGO (66%) (see Table 1). After the long-term cyclic voltammetry scan experiments, the Pt/ZrO<sub>2</sub>-ERGO electrocatalysts were immersed in deionized water for about 1 week after which the methanol oxidation experiment was performed again. Excellent catalytic activity for methanol oxidation was obtained, indicative of the good long-term stability and storage properties of the as-prepared Pt/ZrO<sub>2</sub>-ERGO electrocatalysts.

Fig. 5B shows the polarization and performance curves of the direct methanol fuel cell assembled with the Pt/ZrO<sub>2</sub>-ERGO electrocatalyst as the anode and the commercial Pt/C as the cathode. The cell was operated at 30 °C in the presence of 1 M HClO<sub>4</sub> + 1 M CH<sub>3</sub>OH aqueous solutions. Here, Nafion 112 was used as the membrane. The modified Pt/ZrO<sub>2</sub>-ERGO electrode provided better power performance, by as much as 125 mW cm<sup>-2</sup>, compared to the commercial Pt/C (80 mW cm<sup>-2</sup>). The improved performance can be attributed to the high oxygen reduction activity and the enhanced tolerance towards the oxidation of methanol transferred from the anode to the cathode through the Nafion membrane. In addition, the open-circuit voltage ( $V_{OC}$ ) of Pt/ZrO<sub>2</sub>-ERGO was higher than that of Pt/C. The  $V_{OC}$  of the methanol fuel cell was approximately 0.68 V, with a maximum power density of 125 mW cm<sup>-2</sup> achieved. Further research is underway to improve the power density of the assembled direct methanol cell. The above results indicate that the Pt/ZrO<sub>2</sub>-ERGO composite and the Pt/C composite are excellent platforms for the development of direct methanol fuel cells.

## 4. Conclusion

In summary, we have demonstrated that Pt particles can be deposited on a ZrO<sub>2</sub>-ERGO composite using a very simple electrodeposition method. ERGO is shown to be a good candidate for electrocatalyst support because of its high surface area and high electrochemical performance. The Pt/ZrO<sub>2</sub>-ERGO modified film exhibited better catalytic activity and stability for the electrooxidation of methanol than did the Pt/ERGO modified film, making it a promising choice for efficient electrocatalysts in DMFCs. Furthermore, our approach can be extended to the preparation of other ZrO<sub>2</sub>/Pt based particles on ERGO for electrocatalysis or electrochemical sensors. These Pt/ZrO<sub>2</sub>-ERGO materials demonstrated highly stable performance with greatly enhanced tolerance to electrocatalyst poisoning, and better catalytic activity than other electrocatalysts or Pt-based commercial electrocatalysts. Finally, based on these results, we conclude that the Pt/ZrO<sub>2</sub>-ERGO modified film provides a promising and less expensive alternative to using a methanol oxidation anode electrocatalyst, which is helpful for easy electrooxidation.

## Acknowledgements

The authors would like to express their appreciation for the financial support received from the Ministry of Science and Technology, Taiwan (Republic of China).

## References

- 1 R. Service, *Science*, 2002, **296**, 1222–1224.
- 2 C. Y. Wang, *Chem. Rev.*, 2004, **104**, 4727–4766.
- 3 L. Gao, L. Ding and L. Fan, *Electrochim. Acta*, 2013, **106**, 159–164.
- 4 B. Y. Xia, H. B. Wu, X. Wang and X. W. Lou, *J. Am. Chem. Soc.*, 2012, **134**, 13934–13937.
- 5 H. C. He, P. Xiao, M. Zhou, F. L. Liu, S. J. Yu, L. Qiao and Y. H. Zhang, *Electrochim. Acta*, 2013, **88**, 782–789.
- 6 J. Dong and E. K. Wang, *ACS Nano*, 2010, **4**, 547–555.
- 7 J. Feng, Q. Zhang, A. Wang, J. Wei, J. Chen and J. Feng, *Electrochim. Acta*, 2014, **142**, 343–350.
- 8 Z. Ji, X. Shen, G. Zhu, K. Chen, G. Fu and L. Tong, *J. Electroanal. Chem.*, 2012, **682**, 95–100.
- 9 Y. Lei, B. Liu, J. Lu, R. J. Lobo-Lapidus, T. Wu, H. Feng, X. Xia, A. U. Mane, J. A. Libera and J. P. Greeley, *Chem. Mater.*, 2012, **24**, 3525–3533.
- 10 A. K. Geim and K. S. Novoselov, *Nat. Mater.*, 2007, **6**, 183–191.
- 11 A. T. E. Vilian, S. Chen, Y. Chen, M. Ajmal Ali and F. M. A. Al-Hemaid, *Colloids Surf.*, 2014, **423**, 33–40.
- 12 G. Shi, Z. Wang, J. Xia, S. Bi, Y. Li, F. Zhang, L. Xia, Y. Li, Y. Xia and L. Xia, *Electrochim. Acta*, 2014, **142**, 167–172.
- 13 L. Dong, R. Gari, Z. Li, M. M. Craig and S. Hou, *Carbon*, 2010, **48**, 781–787.
- 14 T. Q. Xu, Q. L. Zhang, J. N. Zheng, Z. Y. Lv, J. Wei, A. J. Wang and J. J. Feng, *Electrochim. Acta*, 2014, **115**, 109–115.
- 15 Y. M. Li, L. H. Tang and J. H. Li, *Electrochem. Commun.*, 2009, **11**, 846–849.
- 16 S. Yu, Q. Liu, W. Yang, K. Han, Z. Wang and H. Zhu, *Electrochim. Acta*, 2013, **94**, 245–251.
- 17 K. Sato, H. Abe and S. Ohara, *J. Am. Chem. Soc.*, 2010, **132**, 2538–2539.
- 18 R. Sandoval, A. M. Cooper, K. Aymar, A. Jain and K. Hristovski, *J. Hazard. Mater.*, 2011, **193**, 296–303.
- 19 J. S. Wang, J. Y. Xi, Y. X. Bai, Y. Shen, J. Sun, L. Q. Chen, W. T. Zhu and X. P. Qiu, *J. Power Sources*, 2007, **164**, 555–560.
- 20 F. Lupo, R. Kamalakaran, C. Scheu, N. Grobert and M. Ruhle, *Carbon*, 2004, **42**, 1995–1999.
- 21 D. J. Guo, X. P. Qiu, W. T. Zhu and L. Q. Chen, *Appl. Catal., B*, 2009, **89**, 597–601.
- 22 R. Liang, M. Deng, S. Cui, H. Chen and J. Qiu, *Mater. Res. Bull.*, 2010, **45**, 1855–1860.
- 23 Y. Shan and L. Gao, *Nanotechnology*, 2005, **16**, 625–630.
- 24 D. C. Marcano, D. Kosynkin, J. M. Berlin, A. Sinititskii, Z. Sun, A. Slesarev, L. B. Alemany, W. Lu and J. M. Tour, *ACS Nano*, 2010, **4**, 4806–4814.
- 25 B. G. Choi, H. S. Park, M. H. Yang, Y. M. Jung, S. Y. Lee, W. H. Hong and T. J. Park, *Nanoscale*, 2010, **2**, 2692–2697.
- 26 Y. Xu, H. Bai, G. Lu, C. Li and G. Shi, *J. Am. Chem. Soc.*, 2008, **130**, 5856–5857.
- 27 Y. Li, K. Sheng, W. Yuan and G. Shi, *Chem. Commun.*, 2013, **49**, 291–293.
- 28 Q. Wu, Y. X. Xu, Z. Y. Yao, A. R. Liu and G. Q. Shi, *ACS Nano*, 2010, **4**, 1963–1970.
- 29 C. J. Cai, M. W. Xu, S. J. Bao, C. Lei and D. Z. Jia, *RSC Adv.*, 2012, **2**, 8172–8178.
- 30 Z. Sun, Z. Rong, Y. Wang, Y. Xia, W. Du and Y. Wang, *RSC Adv.*, 2014, **4**, 1874–1878.
- 31 A. A. Ensafi, M. Jafari-Asl and B. Rezaei, *Electrochim. Acta*, 2014, **130**, 397–405.
- 32 G. Girishkumar, M. Rettker, R. Underhille, D. Binz, K. Vinodgopal and P. Mcginn, *Langmuir*, 2005, **21**, 8487–8494.
- 33 L. A. Estudillo-Wong, A. M. Vargas-Gómez, E. M. Arce-Estrada and A. M. Robledo, *Electrochim. Acta*, 2013, **112**, 164–170.
- 34 W. Ye, Y. Chen, Y. Zhou, J. Fu, W. Wu, D. Gao, F. Zhou, C. Wang and D. Xue, *Electrochim. Acta*, 2014, **142**, 18–24.
- 35 L. Dong, R. Gari, Z. Li, M. M. Craig and S. Hou, *Carbon*, 2010, **48**, 781–787.
- 36 Y. Li, W. Gao, L. Ci, C. Wang and P. M. Ajayan, *Carbon*, 2010, **48**, 1124–1130.
- 37 C. Ma, W. Liu, M. Shi, X. Lang, Y. Chu, Z. Chen, D. Zhao, W. Lin and C. Hardacre, *Electrochim. Acta*, 2013, **114**, 133–141.
- 38 Z. Li, L. Zhang, X. Huang, L. Ye and S. Lin, *Electrochim. Acta*, 2014, **121**, 215–222.
- 39 S. Yu, Q. Liu, W. Yang, K. Han, Z. Wang and H. Zhu, *Electrochim. Acta*, 2013, **94**, 245–251.